30th International Congress on Sound and Vibration

ICSV30 AMSTERDAM 8-11 JULY 2024

REALTIME CONTROL OF THE REFLECTED SOUND FIELD IN A SMALL-SCALE ACTIVE ANECHOIC CHAMBER

R. Haasjes
University of Twente, Drienerlolaan 5, Enschede, 7522 NG, The Netherlands.
E-mail: r.haasjes@utwente.nl
A.P. Berkhoff
University of Twente, Drienerlolaan 5, Enschede, 7522 NG, The Netherlands.
TNO Acoustics and Sonar, Oude Waalsdorperweg 63, The Hague 2597 AK, The Netherlands.
E-mail: a.p.berkhoff@utwente.nl

This paper presents the results of suppressing the acoustic reflections in a 2-dimensional setup using an active control system. The reflected sound field, a non-measurable quantity, is computed with the Kirchhoff-Helmholtz integral, using the particle velocity and the acoustic pressure at the contour. The setup is equipped with 12 primary sources, generating independent disturbance signals, 12 secondary sources, 36 microphones to estimate the particle velocity and measure the acoustic pressure and 3 verification microphones to evaluate the effectiveness of suppressing the reflections. Realtime control is applied in the 60-600 Hz frequency range.
Keywords: Anechoic chamber, Kirchhoff-Helmholtz integral, Active noise control, Reverberation

1. Introduction

Acoustic anechoic chambers are commonly used for applications such as transfer function measurements, sensor calibration, certification of machinery and more [1, 2, 3]. However, especially in the low-frequency range, reflections do exist. Active control is effective in the lower frequency-range. The motivation of this work is to extend the operable frequency-range of existing acoustic anechoic chambers [4, 5], by complementing the passive absorption methods with an active control system. In order to apply active control to suppress reflections from the walls, an estimation of the reflected sound field must be obtained. The reflected sound field is a non-measurable quantity, but methods to obtain an estimation have been proposed [6, 7, 8]. A strategy that computes the reflected sound field with the Kirchhoff-Helmholtz integral is presented in [9], however, the effectiveness of the method is shown with a simulation, without verification on a real-world application. In this work, the Kirchhoff-Helmholtz integral method is applied on a real-world small-scale 2-dimensional setup. In order to compute the Kirchhoff-Helmholtz integral, sensors that are equipped with three microphones in radial direction, are placed on a circle. The signals obtained from the Kirchhoff-Helmholtz integral are subsequently minimized by the control algorithm. An extensive version of the work in this conference paper is submitted as a journal paper [10].

2. The feedforward control setup

A block diagram of a feedforward active noise control system is shown in Fig. 1. In this scheme, the primary noise signal is denoted by $\mathbf{d}(n)$, which is of dimensions L-by-P, in which L denotes the number

of error sensors, P denotes the number of primary sources and n denotes the sample number. The goal of the system is to minimize $\mathbf{e}(n) = \mathbf{d}(n) + \mathbf{y}(n)$, in which $\mathbf{y}(n)$ is the secondary signal. The secondary signal is the control output signal $\mathbf{u}(n)$ filtered by the secondary path $\mathbf{G}(z)$, which is of dimensions L-by-M in which M denotes the number of secondary sources and z denotes the unit-delay forward shift operator. The control filter coefficients $\mathbf{W}(z)$ of dimensions M-by-K, in which K denotes the number of reference sensors, generate the control output signal after filtering with the reference signal $\mathbf{x}(n)$ of dimensions K-by-P.

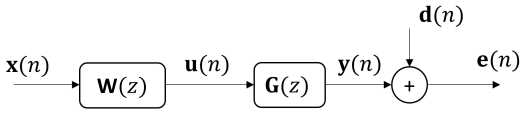

Figure 1: Block-scheme of a feedforward active noise control system [11].

Skipping the mathematics, the set of optimal control filters is found by solving the system of linear equations [11]:

$$\mathbf{w}_{opt}(z) = -\{E[\mathbf{R}^T(n)\mathbf{R}(n)]\}^{-1}E[\mathbf{R}^T(n)\mathbf{d}(n)], \tag{1}$$

in which $\mathbf{R}(n)$ is the matrix of filtered error signals and $E[\cdot]$ denotes the expectation operator. The matrix to be inverted has a Toeplitz-block structure, which can efficiently be solved using block circulant preconditioning with the Conjugate Gradient (PCG) algorithm [12]. A description of the algorithm is presented in [10].

3. Computation of the reflected sound field using the Kirchhoff-Helmholtz integral

The Kirchhoff-Helmholtz integral is computed to obtain the reflected sound field. The full derivation, starting from the acoustic wave equation and the Green's integral theorem can be found in [9]. Using a circular geometry, as shown in Fig. 2, the governing discretized equation is written as [13]:

$$p(\mathbf{x},\omega) = \frac{-jk}{4}\sum_{i=1}^{N_L}(j\rho c V_n(\mathbf{x}_s^i,\omega)H_0^{(2)}(k|\mathbf{x}-\mathbf{x}_s^i|) + p(\mathbf{x}_s^i,\omega)\frac{\mathbf{x}-\mathbf{x}_s}{|\mathbf{x}-\mathbf{x}_s|}H_1^{(2)}(k|\mathbf{x}-\mathbf{x}_s^i|)\cdot\mathbf{n})R\Delta\theta, \tag{2}$$

in which $j = \sqrt{-1}$, ρ is the density of the acoustic medium, c is the speed of sound, $V_n(x_s,\omega)$ is the particle velocity on the surface in the normal inward direction, $H_a^{(b)}$ denotes the Hankel function of kind b and order a, $\mathbf{n}$ is the unit normal inward vector on the surface and $\Delta\theta$ is the angle between the sensors on the surface, assuming the sensors are equidistantly distributed. The particle velocity in the radial inward direction is obtained following [14, 9]:

$$V_n(\mathbf{x}_s^i,\omega) = \frac{p(r_{s+h}^i,\omega) - p(r_{s-h}^i,\omega)}{2jh\omega\rho}, \tag{3}$$

in which h is the distance between the sensors in radial direction, $r_{s-h}^i = ||\mathbf{x}_s^i|| - h$ and $r_{s+h}^i = ||\mathbf{x}_s^i|| + h$ (in polar coordinates).

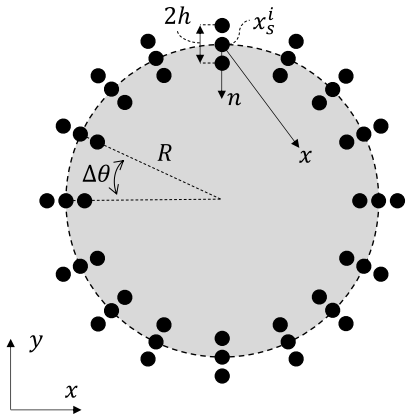

Figure 2: Geometry used for the discretization of the Kirchhoff-Helmholtz integral in case of a circular microphone array [9].

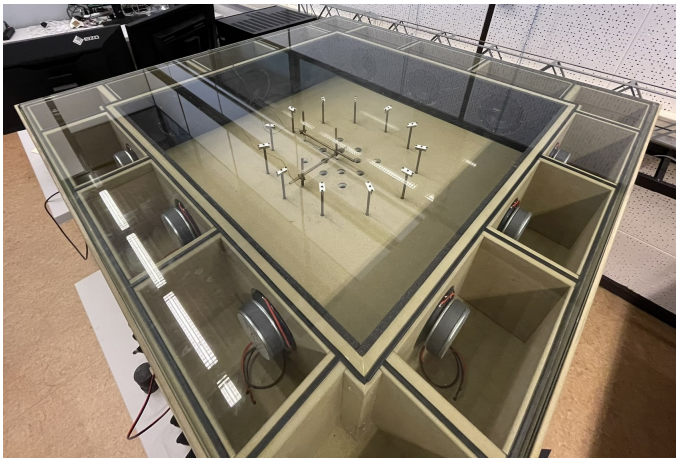

(a) Top view showing the sensor configuration and the secondary sources.

(b) The primary sources connected to the bottom of the experimental setup using tubes.

Figure 3: The experimental setup at the University of Twente.

4. Real-time control on a small-scale anechoic chamber

The experimental setup is shown in Fig. 3(a). The dimensions of the acoustic domain are (L,W,H) 0.84-by-0.84-by-0.20 m. By limiting the height of the acoustic domain to 20 cm, the sound field is considered 2-dimensional up to about 850 Hz, while the frequency range of interest is up to 600 Hz. The setup consists of 12 independent secondary sources placed at the edge, and 12 independent primary sources, which are connected via tubes with a length of 1 m to the center of the setup, as shown in Fig. 3(b).

The setup is equipped with 36 microphones, resulting in 12 sensors containing three microphones aligned in radial direction. The microphones in radial direction are spaced with a distance $h = 1.6$ cm. The reference sensors measure the reference signals using the 12 inner microphones. With the inner and outer microphones on the circle, the particle velocity is estimated. With the middle microphones on the circle the acoustic pressure is measured. Using the acoustic pressure and the particle velocity at the circle, the Kirchhoff-Helmholtz integral is computed. With the Kirchhoff-Helmholtz integral, the transfer

functions at 21 performance sensors are computed. These performance sensors are equally distributed within the circle, as shown in Fig. 4. The setup contains 3 verification sensors, of which the locations are shown in Fig. 4. The verification sensors are used to verify whether the reflections are removed within the circle.

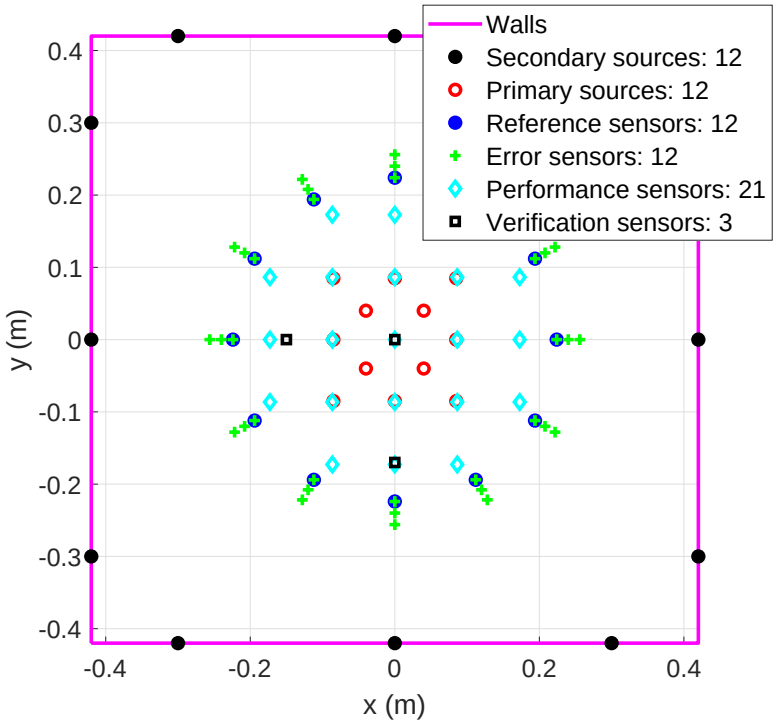

Figure 4: 2-Dimensional schematic view of the experimental setup [10].

All microphones are individually calibrated using an Acoustical Calibrator Type 4231, at 94 dB 1000 Hz. The controller is a Speedgoat machine with multiple IO135 modules, interconnected via their digital ports for synchronization. The system runs at a sampling frequency of $f_s = 5$ kHz. The reference signals are filtered by a high-pass filter having a cutoff frequency at 20 Hz. The error signals are filtered by a low-pass filter having a cutoff frequency at 600 Hz, and a high-pass filter with a cutoff frequency at 60 Hz. The sources generate a logarithmic sweep from 20 to 600 Hz to identify the system. The signals of the performance sensors are minimized by the control algorithm. The controller filter coefficients with a length of $I = 250$ samples are computed using the PCG time-domain algorithm. During control, the primary sources generate independent logarithmic sweeps from 20 to 600 Hz, which are randomly varied in duration and starting time.

The spectral density of the first four performance signals measured at the performance sensor locations is shown in Fig. 6(a). This shows that the controller reduces the signals as computed by the Kirchhoff-Helmholtz integral up to about 600 Hz by an average of 9.6 dB. The spectral density of the signals measured by the verification sensors is shown in Fig. 6(b), from this figure can be seen that the spectral density becomes increasingly flat, i.e. the resonances have been suppressed and an average reduction in the total sound pressure level of 4.4 dB is achieved.

Figure 5: Spectral densities of the signals after running the realtime system.

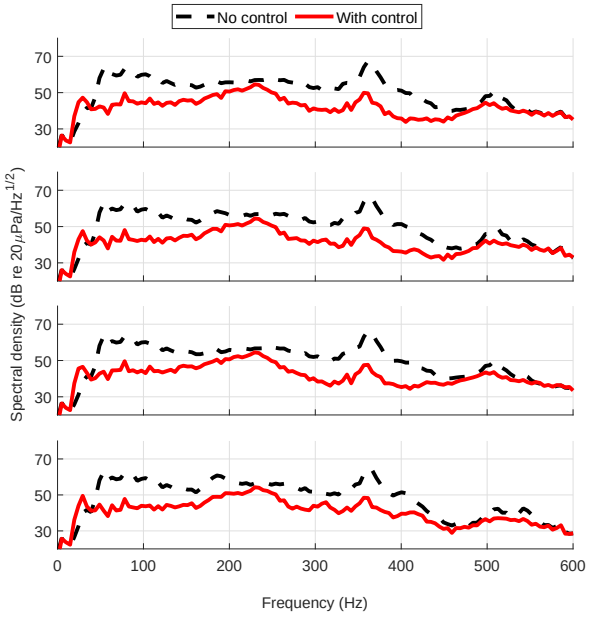

(a) Spectral densities of the signals of the first four performance sensors [10]. The reduction levels from top to bottom respectively are 8.9, 10.2, 9.7 and 9.7 dB.

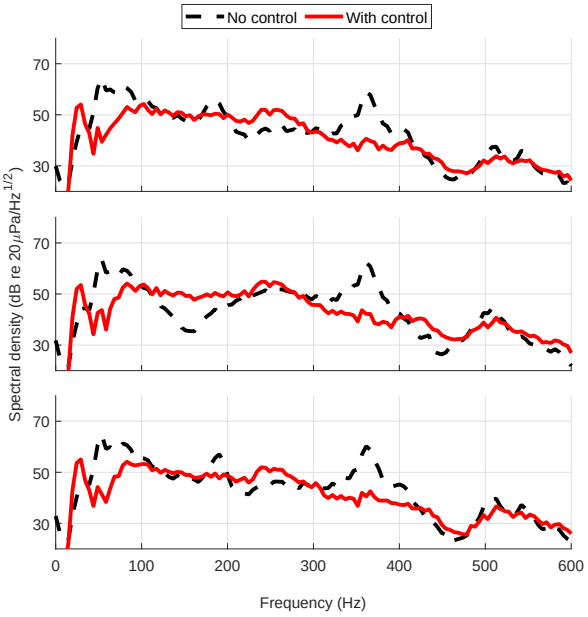

(b) Spectral density of the signals measured by the verification sensors [10]. The reduction levels from top to bottom respectively are 4.7, 3.6 and 5.0 dB.

5. Conclusions

The realtime control of reflections in a 2-dimensional sound field is shown. The inward-traveling sound waves are computed using the Kirchhoff-Helmholtz integral in combination with 12 sensor triplets on a circle, each aligned in radial direction. An average reduction of reflections of 9.6 dB over all performance sensors is achieved. The performance is evaluated using verification sensors within the circle. The spectral densities show that the resonances have been suppressed using the active control system. The sound pressure at the verification sensors is reduced by an average of 4.4 dB.

6. Acknowledgments

This research is funded by TNO. The support and funding from TNO are gratefully acknowledged. The authors would like to thank Henny Kuipers for the design of the custom pre-amplifier hardware and Axel Lok for the help with facilitating and assembling the experimental setup and calibration of the microphones.

REFERENCES

1. V.F. Kopiev, V.V. Palchikovskiy, I.V. Belyaev, Yu. V. Bersenev, S. Yu. Makashov, I.V. Khramtsov, I.A. Korin, E.V. Sorokin, and O. Yu. Kustov. Construction of an anechoic chamber for aeroacoustic experiments and examination of its acoustic parameters. *Acoustical Physics*, 63(1):113 124, 2017.

2. B. D. Patchett and B. E. Anderson. Nonlinear characteristics of high amplitude focusing using time reversal in a reverberation chamber. *Journal of the Acoustical Society of America*, 151(6):3603 3614,

2022.

3. K. Sozanski and A. Sozanska. Low frequency loudspeaker measurements using an anechoic acoustic chamber. In *2018 Signal Processing: Algorithms, Architectures, Arrangements, and Applications (SPA)*, page 367 372, Poznan, Poland, 2018.

4. S. Schneider and C. Kern. Acoustical behavior of the large anechoic chamber at the laboratoire de Mécanique et d'Acoustique in the low frequency range. *Acta Acustica united with Acustica*, 94:141–147, 01 2008.

5. I.V. Belyaev, A. Yu. Golubev, A. Ya. Zverev, S. Yu. Makashov, V.V. Palchikovskiy, A.F. Sobolev, and V.V. Chernykh. Experimental investigation of sound absorption of acoustic wedges for anechoic chambers. *Acoustical Physics*, 61(5):606 614, 2015.

6. D. Habault, E. Friot, Ph. Herzog, and C. Pinhede. Active control in an anechoic room: Theory and first simulations. *Acta Acustica united with Acustica*, 103:369–378, 2017.

7. E. Friot, R. Guillermin, and M. Winninger. Active control of scattered acoustic radiation: a real-time implementation for a three-dimensional object. *Acta Acustica united with Acustica*, 92:278–288, 2006.

8. E. Friot and C. Bordier. Real-time active suppression of scattered acoustic radiation. *Journal of Sound and Vibration*, 278(3):563 580, 2004.

9. R. Haasjes and A.P. Berkhoff. An efficient offline scheme to compute an fir controller for active reduction of acoustic reflections in an anechoic chamber. *Journal of Sound and Vibration*, 573:118198, 2024.

10. R. Haasjes and A.P. Berkhoff. A small-scale active anechoic chamber. *Applied Acoustics*, 2024, Submitted.

11. S.J. Elliott. *Signal Processing for Active Control*. Signal Processing and its Applications. Academic Press, California, USA, 2001.

12. T.F. Chan and J.A. Olkin. Circulant preconditioners for Toeplitz-block matrices. *Numberical Algorithms*, 6:89 – 101, 1992.

13. Edo Hulsebos, Diemer de Vries, and Emmanuelle Bourdillat. Improved microphone array configurations for auralization of sound fields by wave-field synthesis. *J. Audio Eng. Soc*, 50(10):779–790, 2002.

14. Paolo Peretti, Stefania Cecchi, Laura Romoli, and Francesco Piazza. Performance evaluation of adaptive algorithms for wave field analysis/synthesis using sound field simulations. In *Computational Simulations and Applications*, chapter 25, pages 543–560. IntechOpen, Rijeka, Croatia, 2011.